UNCLASSIFIED: Dist A. Approved for public release

Development of a Blast Event Simulation Process for Multi-Scale Modeling of Composite Armor for Light Weight Vehicles

John P. Kim, Nickolas Vlahopoulos
University of Michigan

Geng Zhang
Michigan Engineering Services, LLC

ABSTRACT: This paper presents the development of a multi-scale simulation process for modeling the response of a vehicle with composite armor to the blast loads from an explosive threat. The new process can be used for improving the blast resistant capabilities of the composite armor by configuring its properties at the micro-level. A Blast Event Simulation system (BEST) that facilitates the easy use of LS-DYNA or ABAQUS for conducting a complete sequence of explosive simulations and the inclusion of Anthropometric Test Device (ATD) comprises one of the two main foundation components of the new development. The Micromechanics Analysis Code (MAC) developed by NASA Glenn comprises the second main foundation component. Details from a validation study of BEST associated with the response of a generic structure and an ATD placed inside it to an explosion are discussed. The development of the new multi-scale simulation capability is discussed and a case study is presented. The case study demonstrates how the new simulation approach can determine a matrix-fiber configuration and the orientation of the laminates at the micro-level for designing blast resistant composite armor that offers similar levels of protection with steel but at significantly reduced weight.

Keywords: Light weight vehicles; survivability; Blast Event Simulation system; Anthropometric Test Device; Multi-scale modeling; Composites; Matrix-fiber configuration;

Reference to this paper should be made as follows: John, P.K., Nickolas, V. and Geng, Z. (2011) 'Development of a Blast Event Simulation Process for Multi-Scale Modeling of Composite Armor for Light Weight Vehicles', Int. J. Vehicle Design, Vol. xx, No. x, pp.xx-xx

Biographical notes: Biographical notes

Report Documentation Page

Form Approved
OMB No. 0704-0188

Public reporting burden for the collection of information is estimated to average 1 hour per response, including the time for reviewing instructions, searching existing data sources, gathering and maintaining the data needed, and completing and reviewing the collection of information. Send comments regarding this burden estimate or any other aspect of this collection of information, including suggestions for reducing this burden, to Washington Headquarters Services, Directorate for Information Operations and Reports, 1215 Jefferson Davis Highway, Suite 1204, Arlington VA 22202-4302. Respondents should be aware that notwithstanding any other provision of law, no person shall be subject to a penalty for failing to comply with a collection of information if it does not display a currently valid OMB control number.

1. REPORT DATE	2. REPORT TYPE	3. DATES COVERED
15 MAR 2011	**N/A**	**-**

4. TITLE AND SUBTITLE	5a. CONTRACT NUMBER
Development of a Blast Even Simulation Process for Multi-Scale Modeling of Composite Armor for Light Weight Vehicles (PREPRINT)	**W56HV-04-2-0001**
	5b. GRANT NUMBER
	5c. PROGRAM ELEMENT NUMBER
6. AUTHOR(S)	5d. PROJECT NUMBER
John P. Kim; Nicholas Vlahopoulos; Geng Zhang	5e. TASK NUMBER
	5f. WORK UNIT NUMBER
7. PERFORMING ORGANIZATION NAME(S) AND ADDRESS(ES)	8. PERFORMING ORGANIZATION REPORT NUMBER
University of Michigan Michigan Engineering Services, LLC	
9. SPONSORING/MONITORING AGENCY NAME(S) AND ADDRESS(ES)	10. SPONSOR/MONITOR'S ACRONYM(S)
US Army RDECOM-TARDEC 6501 E 11 Mile Rd Warren, MI 48397-5000, USA	**TACOM/TARDEC/RDECOM**
	11. SPONSOR/MONITOR'S REPORT NUMBER(S) **21550**

12. DISTRIBUTION/AVAILABILITY STATEMENT
Approved for public release, distribution unlimited

13. SUPPLEMENTARY NOTES
Submitted for publication in a Special Issue of Int'l Journal of Vehicle Design, The original document contains color images.

14. ABSTRACT

15. SUBJECT TERMS

16. SECURITY CLASSIFICATION OF:			17. LIMITATION OF ABSTRACT	18. NUMBER OF PAGES	19a. NAME OF RESPONSIBLE PERSON
a. REPORT	b. ABSTRACT	c. THIS PAGE			
unclassified	**unclassified**	**unclassified**	**SAR**	**23**	

1 Introduction and problem statement

The design of vehicles to resist a blast and provide protection to the vehicle and its occupants is of great interest. New combat vehicle designs emphasize weight reduction for increased fuel efficiency and airborne transportation; therefore, a significant effort must be invested to ensure that the vehicle's survivability is not compromised. Currently combat vehicles are subjected to blasts from explosive threats. The recent wars in Iraq and Afghanistan have underlined the importance for increasing the protection of a vehicle's occupant to explosions. In addition to the loss of life, either traumatic brain injuries or extremities injuries have been observed [Fischer, 2009; Galarneau et al, 2006]. Weight reduction and high level of survivability are mutually competing objectives. Therefore, significant effort must be invested in order to ensure that the vehicle's survivability is not compromised. Composite materials provide some of the most viable options for manufacturing composite armor that can increase survivability without a significant weight penalty. In this paper a new multi-scale simulation process for modeling the response of composite armor to explosive threats is presented. The development is based on integrating capabilities of the BEST and the MAC software. It enables configuring the composite at the matrix-fiber level for increased blast resistance.

In the past, several efforts have been made for modeling explosions and their effect on structures [Gupta, 1999; Bird, 2001; Gupta, 2002; Sun et al, 2006]. Empirical loading models have been developed for predicting the effects of blast mines on structures. Empirical blast loading functions were implemented in the CONWEP code [Kingery and Bulmarsh, 1984] for modeling the free air detonation of a spherical charge. Another empirical relationship was developed for predicting the impulse applied by a buried mine to a plate at a given offset from the mine [Westine et al, 1985]. Both empirical models were integrated with the LS-DYNA commercial code. The CTH hydrocode [McGlaun et al, 1990; Bell and Hertel, 1994] has been developed by Sandia National Laboratories and utilized for blast event simulations in multiple occasions [Gupta, 1999; Gupta, 2002; Gupta et al, 1987; Gupta et al 1989, Joachin et al, 1999] for modeling blast events. The BEST process for conducting a complete analysis for the explosive/ soil/ vehicle/ occupant interaction has been presented along with validation through comparison to test data (Reference [15], [26]). BEST is utilized in this paper for evaluating the loads from the explosion on the structure and for preparing the LS-DYNA or ABAQUS computations for the vehicle structure.

A micromechanical method of cells, for the analysis of fibrous composites with periodic structure, was developed and verified [Aboudi, 1989; Aboudi, 1991]. Analysis of composites using the Generalized Method of

Cells (GMC) was developed for modeling of multiphase periodic composites. Effective constitutive laws that govern overall behavior of the elastic-viscoplastic composite material were established [Paley and Aboudi, 1992; Aboudi, 1995]. The GMC theory was reformulated for maximum computational efficiency [Bednarcyk and Pindera, 1999; Bednarcyk and Pindera, 2000] and the Integrated multi-scale Micromechanics Analysis Code (ImMAC) was developed by NASA Glenn Research Center. This includes the Micromechanics Analysis Code (MAC) with the generalized method of cells that analyzes the thermo-inelastic behavior of composite materials and laminates [Bednarcyk and Pindera, 2002]. The Explicit solver of ABAQUS is coupled with the MAC code, enabling multi-scale computing from the micro level to the global level. A major advantage of this integrate multi-scale simulation process is that it allows propagating information from the constitutive micro-level like fiber failures, matrix damage, inelasticity, interfacial debonding to the global structural response level. The MAC and the ABAQUS codes exchange information through the homogenization and localization simulation processes. During the homogenization process, the MAC code determines the material response at the integration points within each ABAQUS element. In essence, MAC operates as a nonlinear constitutive model within ABAQUS, representing the heterogeneous material. In reverse, during the localization process, local stress and strains computed by ABAQUS from incrementally applied loading are applied to the MAC for obtaining updated effective material properties (Figure1).The MAC/ABAQUS computational capability comprises the second main foundation component of the new development.

Figure 1 Associated level scales for composite analysis

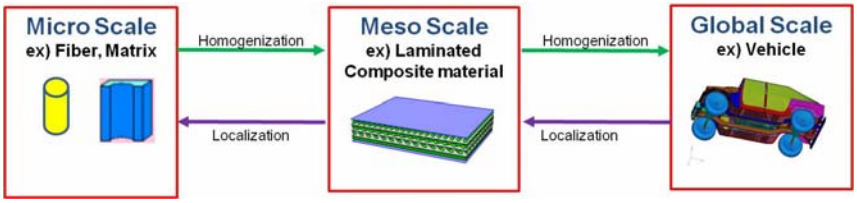

In this paper, through the BEST synthesis tool, the Eulerian solver of LS-DYNA is employed for simulating the soil – explosive – air interaction and calculating accurately the loads on a target structure. Sequentially, the LS-DYNA Langragian solver or the ABAQUS solver coupled with the MAC code is used for computing the corresponding response of a target structure to the loads from the explosion. A major advantage of utilizing the LS-DYNA and ABAQUS solvers for blast event simulations instead of CTH is that LS-DYNA and

ABAQUS are commercially readily accessible codes, have a friendly user interface, can exchange data with commercial pre and post processors, it is easy to interpret the structure of the data files, and numerical models for an ATD can be readily integrated in the simulation as part of the vehicle finite element model.

The BEST is a synthesis tool with built-in knowledge for preparing the various data files required for conducting the blast simulation and ADT analysis. BEST provides a series of templates that guide the user in developing the necessary models for the blast event simulations. A capability has been developed for automatically creating the Eulerian finite element model for the air, the soil, and the explosive, given the structural finite element model for the vehicle. An occupant model of an ATD can be introduced inside the vehicle model, if desired. The effect of moisture in the soil properties is considered during the generation of the soil – explosive – air model used by the Eulerian solver. Tracers are defined in the Eulerian model for all structural finite elements which are on the outer part of the vehicle structure and are subjected to the load from the blast. The data for the pressure load from the explosion comprise the loading for the structural response of the target structure. A methodology has also been developed for using the pressure information from the explosion for assigning appropriate velocity and trajectories to projectiles and fragments that are part of the explosive threat. The projectiles are considered along with the blast pressure load to hit the structure and the response of the structure to the combined loads can be computed.

The BEST simulation process was first validated through comparison with test data available in the literature [Bergeron et al, 1998; Williams and McClennan, 2002] (Reference [15]). Further validation of the BEST process is presented in this paper by analyzing a generic target structure with a V shaped double bottom subjected to a load from an explosion and comparing the results to test data. A Hybrid III ATD is placed inside the structure. A test was conducted for this configuration. Results from the BEST simulation process were compared successfully with test data for the deformation of the structure and for the loads developed in the lower legs of the occupant (Figure 2).

The algorithm and the process utilized for coupling the ABAQUS and MAC codes is discussed. The coupling can be done either in a fully coupled mode or as an one-way-coupling. In the former, at each iteration of each time step, information about the strain field at each integration point of each element is communicated from ABAQUS to MAC. In return, the MAC code computes the constitutive properties and provides their updated values to ABAQUS. In the latter, the MAC code is used for computing the constitutive material properties (assuming no deformation) and provides them as input to the ABAQUS analysis. In order to demonstrate the type of results

obtained by the two coupling approaches a generic target structure with a V shaped outer bottom, subjected to a load from an explosion is analyzed by the one-way-coupling approach and by the fully coupled method. When the one-way-coupling approach is used both the LS-DYNA and the ABAQUS solvers are employed for conducting the vehicle analysis. The fully coupled analysis is conducted using only the ABAQUS solver since the fully coupled mode of operation is only available between MAC and ABAQUS. Further a case study associated with the analysis of a generic all metal structure and a metal-composite structure is presented. It is demonstrated that the new simulation approach can determine a matrix-fiber configuration and the orientation of the laminates at the micro-level in order to maximize the protection offered by the composite armor while reducing the weight.

Figure 2 Comparison between results from BEST and test data for a V shaped double bottom structure and the enclosed occupant

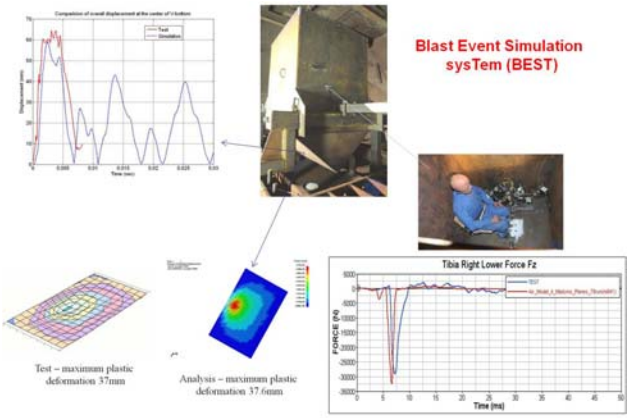

2 Correlation to test data for generic vehicle structure and an ATD

Technical information related with the generic vehicle structure is presented next. No information was received by any Government organization or any prime vehicle manufacturer in designing the generic vehicle structure and the experimental set up. Figure 3 presents the general engineering drawings for the structure. Armox 370H armor steel with 15mm thickness is used for the entire outer V-shaped bottom structure, while 10mm construction steel is used for the inner bottom and all other panels.

Figure 3 Engineering drawings for generic vehicle structure used in validation study of BEST

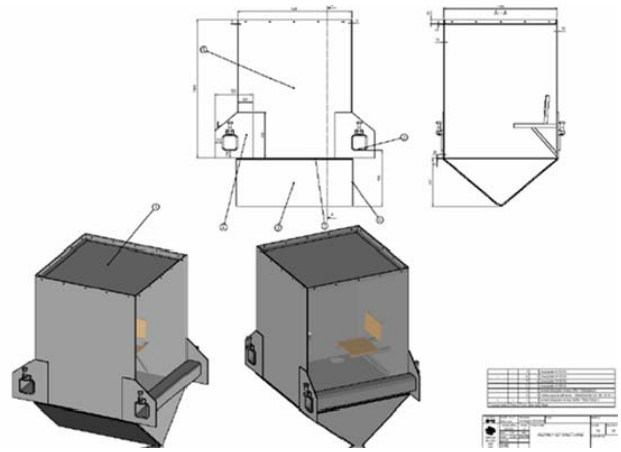

The testing was performed at the test banker facility of TNO Defense, Security, and Safety under a contract issued from Michigan Engineering Services, LLC. Figure 4 presents photos of the facility, the generic vehicle, the Hybrid III dummy placed inside the generic vehicle, and a drawing about the test frame structure. The vehicle structure is held rigidly in place through a heavy support frame. The middle photo in Figure 4 zooms in the support assembly that holds the target vehicle structure in place during the explosion. The explosive is placed inside a steel pod underneath the vehicle and directly in the middle of the bottom. This explosive configuration allows concentrating the power released from the explosion to the target structure. 5.51kg of C4 were utilized during the test.

Figure 4 Generic vehicle structure utilized for validating results from BEST simulations

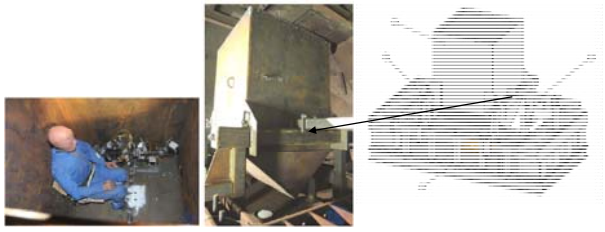

Simulation models developed and utilized by BEST are presented in Figure 5. The combined Eulerian and Langrangian models are presented on the left, while half of the Langrangian structural model is presented in the middle. The Hybrid III simulation model placed inside the generic vehicle is presented on the right side of Figure 5.

Figure 5 Numerical models used for validating results from BEST simulations

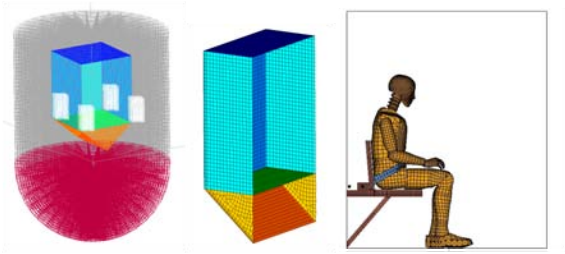

Several comparisons between simulation results and test data were made. The strains were measured at three locations (one out of the four strain gages failed) along the middle of the outer V-shaped bottom. Figure 6 presents the locations of the strain gages and the comparison between test and simulations. Overall good correlation is observed, particularly for the strain gage placed in the middle of the bottom structure, where the highest strain values are encountered. The simulation results cannot capture a large compressive strain which is encountered very early in the test time histories. The measured strains originate from a combination of in-plane compressive deformation and out-of-plane bending deformation. It is assessed that the high compressive strains which appear early in the test results originate from the high speed compressive wave which reaches the strain gages early in the process, while the remaining strains which are captured correctly from the simulations correspond to the bending deformation of the bottom structure.

The displacement time histories in the middle of the inner floor structure and in the middle of the outer V-shaped bottom structure were also measured using high speed cameras. The placement of the cameras and the correlation between simulation results and test is presented in Figure 7. Very good correlation is observed for both the outer bottom structure and the inner floor structure. The high speed camera measuring the displacement on the outer bottom structure failed after the initial part of the measurements, but likely the early stage was recorded when the high response is exhibited. Permanent deformation is induced in the outer bottom structure in both test and simulation, while the inner floor remains within the elastic region in both measurements and simulation. The permanent deformation induced on one of the two sections of the V-shaped outer bottom structure is measured and compared to the simulation results in Figure 8. Since the structure is symmetric and a symmetric explosive was placed at the plane of symmetry, the results are the same for the two sections of the outer bottom structure. Very good correlation is observed for the deformation pattern between the test and the simulations. The comparison for the maximum permanent deformation encountered in the bottom structure is also very good.

Figure 6 Locations of strain gages on outer V-shaped bottom structure and comparison between test results and BEST simulations

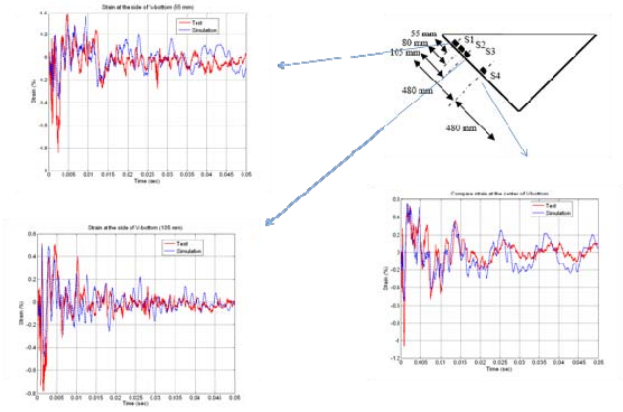

Figure 7 Locations of displacement histories measurements on and outer V-shaped bottom structure (left) and inner floor (right); comparison between test results and BEST simulations

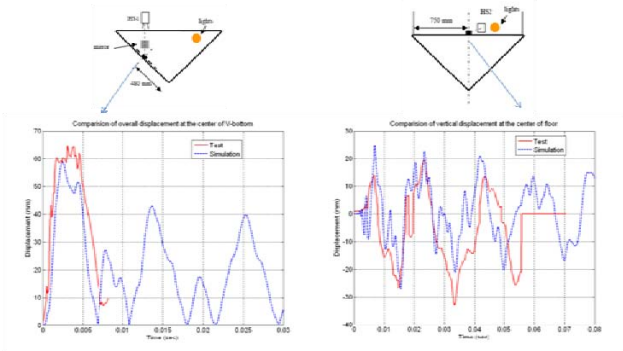

Figure 8 Comparison between test results and BEST simulation of the permanent deformation induced in one of the two sections of the outer V-shaped bottom structure

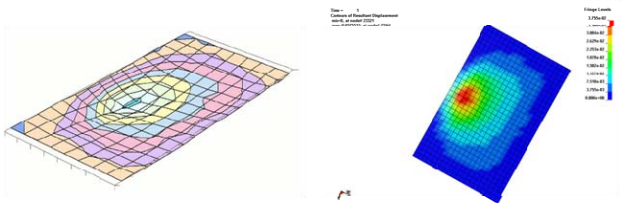

Test – maximum permanent deformation 37mm

Analysis – maximum permanent deformation 37.6mm

In the final step of the correlation study, results between test and BEST are compared for the right and the left leg of the occupant. The forces in the vertical z-direction and in the forward/back x-direction at the lower and upper tibia of the right and the left legs are compared with measurements. Results for the right leg are presented in Figure 9, while results for the left leg are presented in Figure 10 (for the left leg the measurements failed for the upper tibia). Good correlation is observed in capturing the maximum forces which are developed in the lower extremities of the occupant. It is worth mentioning that all existing ATD models have been developed for automotive crash testing, thus, the embedded measurement capabilities and the corresponding simulation models have been geared towards operating properly in the time scales encountered in automotive crashes. The time scales encountered in explosive events are of much shorter duration and this must be considered when comparing measurements and simulations. Therefore, it is also useful to further compare the kinematic behavior of the ATDs between test and simulation in addition to the absolute values of the forces. Such comparison between the BEST results and the recorded motion from test is presented in Figure 11. The good correlation which is observed in Figure 11 further demonstrates the feasibility of using BEST simulation technology for modeling the response of a vehicle's occupant to a blast.

Figure 9 Comparison between BEST results and test data for the forces developed on the right tibia

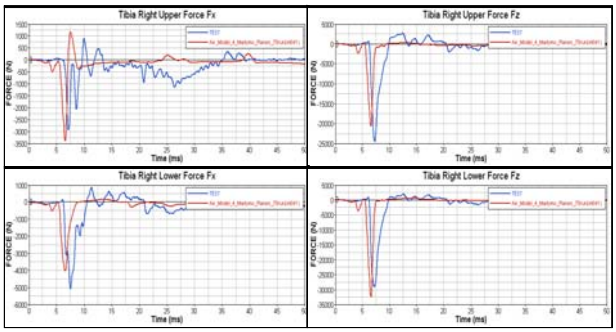

Figure 10 Comparison between BEST results and test data for the forces developed on the left leg

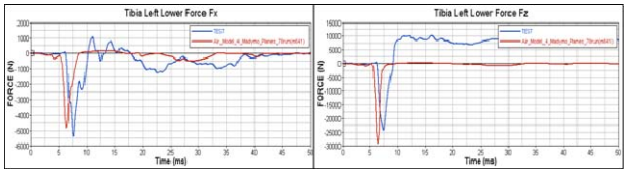

Figure 11 Comparison of the kinematic response of the ATD between BEST simulations and test for various time instances

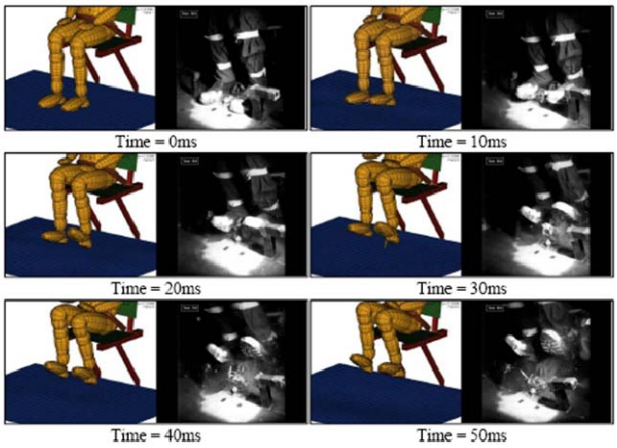

3 Background on MAC code and the fully coupled ABAQUS-MAC solution sequence

Basic theory of the Generalized Method of Cells (GMC), forms the foundation of MAC code. This information is discussed in detail in reference [20] and briefly presented here. The GMC is considering a repeating volume-element of a multiphase unidirectional fibrous composite with a periodic structure as the one depicted in Figure 12-(a). This typical repeating volume-element consists of N_β * N_λ sub-cells and each of these sub-cells is occupied by an elastic-viscoplastic material as Figure. 12-(b). The equivalent continuum medium in which the repeating volume element is represented by the point P as Figure 12-(c) and representative volume element consists of different elastic-viscoplastic materials, i.e., it represents a multiphase inelastic composite material.

Figure 12 Composite possesses a periodic structure that a representative repeating volume element from reference [20].

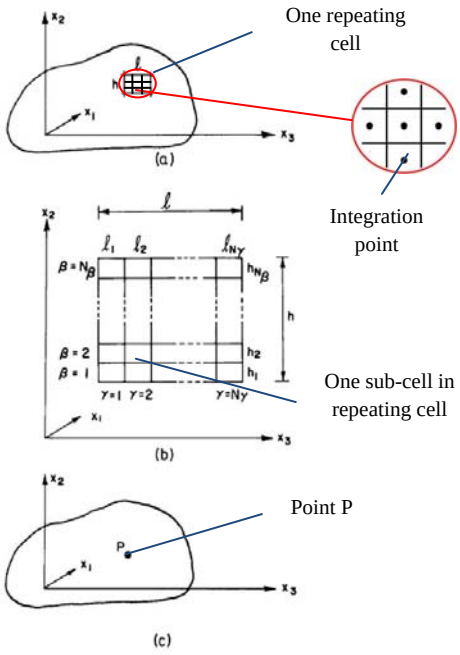

The micromechanical analysis starts by placing a repeating volume element of the periodic multiphase composite, in sequence macroscopic average stresses and strains are defined from the microscopic average stresses. The rate of displacements and tractions continuity conditions at the interfaces between constituents are imposed to eliminate the micro-variables and with micro-equilibrium, the relationship between microscopic strains and macroscopic strains are established through the relevant concentration tensors. Finally a set of continuum equations that model the overall macroscopic behavior of the composite are determined.

The outlined four steps form the basis of micro-to-macromechanics analyses which describe the behavior of heterogeneous media. The resulting micromechanical analysis establishes the overall elastoplastic behavior of the multiphase inelastic composite. This is expressed as an effective elastic-plastic constitutive relation between the average stress, strain, and plastic strain, in conjunction with the effective elastic stiffness tensor B^*. [Suquet, 1985; Paley and Aboudi, 1992]

$$\bar{\tau} = B^{*}(\bar{\eta} - \bar{\eta}^{P}) \tag{1}$$

where the effective elastic stiffness tensor B^* is defined by

$$B^{*} = \frac{1}{hl}\sum_{\beta=1}^{N_\beta}\sum_{\gamma=1}^{N_\gamma} h_\beta l_\gamma C^{(\beta\gamma)} A^{(\beta\gamma)} \tag{2}$$

where h is the sub-cell height, l is the sub-cell length, $C^{(\beta\gamma)}$ is the elastic stiffness tensor of material in each sub-cell. The composite plastic strain-rate tensor for two repeating sub-cells is defined by

$$\bar{\eta} = (\bar{\eta}_{11}, \bar{\eta}_{22}, \bar{\eta}_{33}, 2\bar{\eta}_{23}, 2\bar{\eta}_{13}, 2\bar{\eta}_{12}) \tag{3}$$

$$\bar{\eta}^{P} = -B^{*^{-1}}\sum_{\beta=1}^{N_\beta}\sum_{\gamma=1}^{N_\gamma} h_\beta l_\gamma C^{(\beta\gamma)} \times (A^{P(\beta\gamma)}\eta_S{}^{P} - \bar{\eta}^{P(\beta\gamma)})/(hl)\,. \tag{4}$$

where $\eta_S{}^{P}$ represents the plastic strain-rates vector of the sub-cells. The concentration matrices A and A^P are defined as:

$$A = \begin{bmatrix} A_M \\ A_G \end{bmatrix}^{-1} \bullet \begin{bmatrix} 0 \\ J \end{bmatrix} \tag{5}$$

$$A^P = \begin{bmatrix} A_M \\ A_G \end{bmatrix}^{-1} \bullet \begin{bmatrix} A_M \\ 0 \end{bmatrix} \tag{6}$$

where matrix A_M represents elastic properties of the material at the sub-cell level, matrix A_G represents geometrical properties of the repeating-cell and matrix J represents interfacial properties of two repeating-cells.

The GMC theories implemented within MAC code were reformulated for maximum computational efficiency and for considering deformation history, loading path and loading rate. [Bednarcyk and Pindera, 1999]

The ABAQUS code can be used in two modules of operation, Standard (Implicit) and Explicit. In the standard module, the stress satisfying the constitutive equation is computed first and then a consistent tangent modulus (Jacobian Matrix) is evaluated. Sequential iterations are performed until the stress obtained by the consistent tangent modulus satisfies the constitutive equation. Each increment in this analysis consists of at least one iteration which requires the solution of a set of simultaneous equations. The cost per iteration is roughly proportional to the number of degrees of freedom in the model squared. It is difficult to reach consistent tangent modulus for complex constitutive equation using the implicit solver. Further convergence for abrupt increase or decrease in the loads is deficient. As a result, the standard module is primarily used for monotonic loading and linear or mildly nonlinear problems where nonlinearities are smooth. In the ABAQUS explicit, each increment consists of one group of equations, so there are no iterations and the solution is calculated by explicit time integration step by step. Therefore the maximum increment size is limited in the calculations of the explicit module. As a consequence, the explicit module is primarily used high-speed dynamic events, such as impacts and nonlinear transient analysis. In this paper, explicit module is employed for conducting blast event simulations.

The FEAMAC code comprises a fully coupled simulation process between MAC and the ABAQUS implicit module. FEAMAC consists of ABAQUS/Standard user defined subroutines, as well as subroutines exclusive to the FEAMAC package. Mechanical analysis is achieved through the ABAQUS/Standard subroutine UMAT. For every integration points of each finite element the UMAT subroutine is called by ABAQUS/Standard, and provides the strains, strain increments, and current values of state variables information to the MAC code. The MAC code then returns a new stiffness and stress state to the UMAT via the FEAMAC subroutine (Figure 13).

Figure 13 Flow chart describing coupling between ABAQUS implicit or explicit and MAC

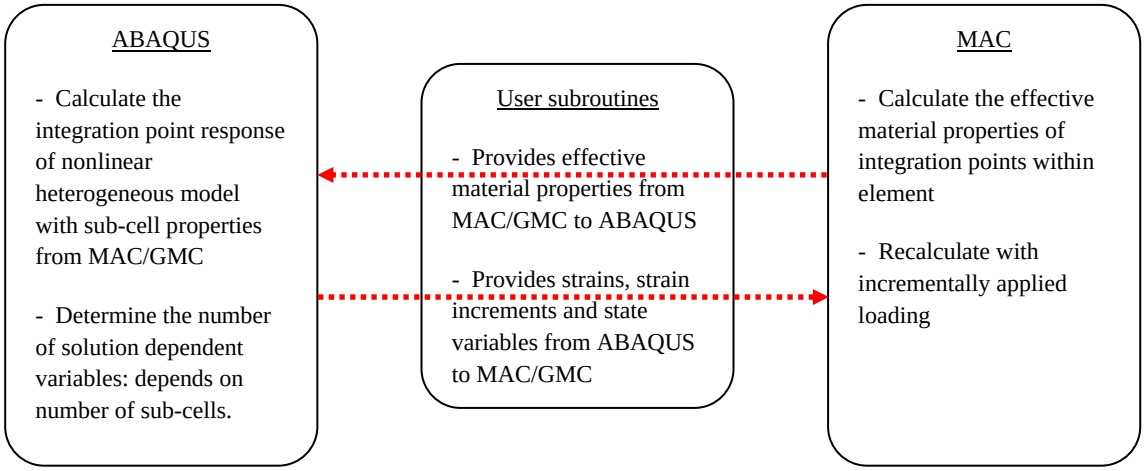

The computational framework of explicit module differs significantly from implicit one, corresponding subroutine VUMAT are desired for blast event simulation as stated above. The user subroutine VUMAT in explicit module uses different arguments. The VUMAT calls for blocks of material calculation points for which the material is defined in a user subroutine and updates the stress states for each material point in the block by looping through all material points in the block, while the UMAT calls at all material calculation points of elements for which the material definition includes a user defined material behavior. Through this difference, VUMAT consists of the one additional column of the material point numbers and the other column from the UMAT arrays. For instance the stress state in UMAT is represented by the vector “STRESS (NTENS)” where “NTENS” is size of the stress component array, number of direct stress components and shear stress components, but stress state in VUMAT is represented by the vector “STRESSNEW (NBLOCK, NDIR+NSHR)” where “NBLOCK” is the material point number of a block and “NDIR+NSHR” is size of the stress component array similar to “NTENS”. In this respect and maintaining existing subroutines to communicate with MAC code, VUMAT subroutine is formatted to interact between existing subroutines and explicit module by updating the stress state for each material point and deformation gradient information and converting them back (Figure 14).

Figure 14 Architecture of coupling between (a) ABAQUS Implicit and MAC; (b) ABAQUS Explicit and MAC

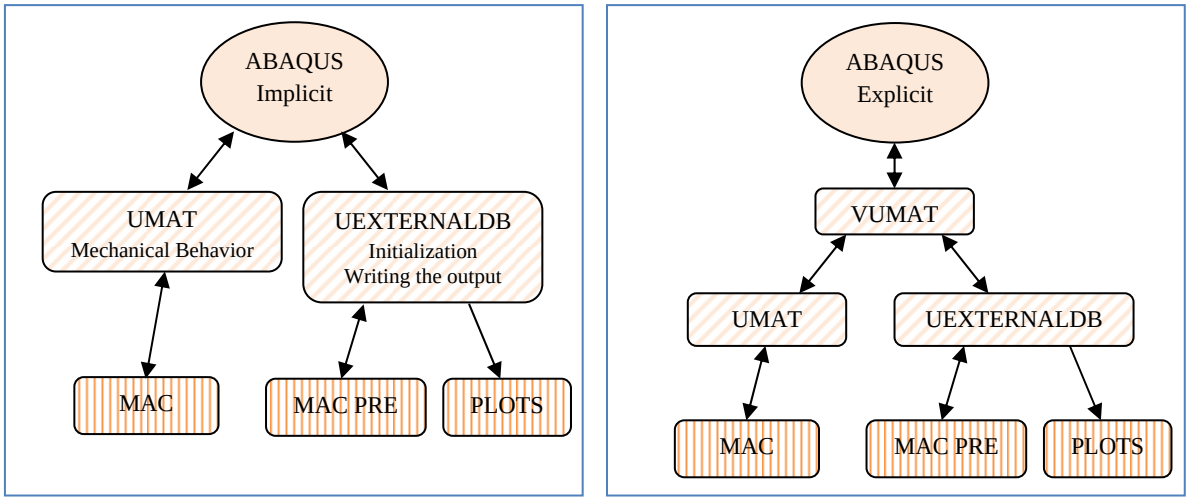

(a) (b)

The formatted frame capacitates to propagate local phenomena of composites, like fiber failures, matrix damage, interfacial debonding, throughout the structural response. This fully coupled multi-scale simulation frame will be used for analyzing blast events.

4 Result of multi-scale simulation case study

A target structure similar to the one used in the experimental validation presented in Section 2 is used for the case study work presented in this Section. The target structure is comprised of a box with a V shaped outer bottom. The numerical finite element model which is used in the simulations is presented in Figure 15. The dimensions of the box are 2m x 2m x 1.8m (1.8m is height), the floor of the box is 0.8m above ground and the tip of the V shaped outer bottom is 0.5m above ground. The roof and four lateral walls have thickness of 0.01m, the inner floor has thickness of 0.02m and the outer V shaped bottom has thickness of 0.03m. The BEST simulation process is used for conducting the Eulerian analysis for the explosive and the air which surrounds the target structure. During this simulation the interface between the vehicle and the air is considered as a rigid boundary. The Eulerian simulation computes the pressure time histories at a number of tracer points placed at the interface between each structural element and the air. During the Eulerian analysis, the interaction between the explosive, the soil and the air is computed and the load histories applied on the structure due to the explosion are computed. The BEST process also has the capability to include a user defined number of projectiles as part of the explosive threat (Reference [26]).

Figure 15 Air-Explosive-Structure model for case study and tracer points

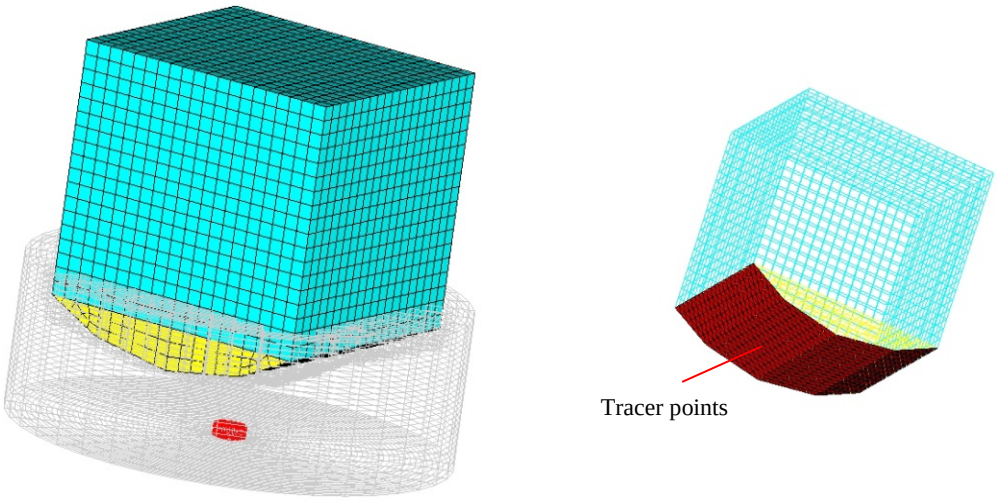

A set of three simulations is conducted first by considering the inner floor and the outer V shaped bottom structure made out of composite material and the rest of the box made out of steel. Titanium matrix composite material, comprised by SiC (SCS Ultra) fiber and Ti-6Al-4V matrix with 60 percent fiber volume fracture for each cell, is used for the inner floor and the outer V shaped bottom structure. The material properties of steel, fiber and matrix are presented in Table 1 & 2. The number, the relative orientation and the thickness of the layers that comprise the composite laminate material are also summarized in Table 1.

Table 1 Material properties of steel

	Steel (Layer 1)	Steel (Layer 2)	(unit)	Composite (Layer 1)	Composite (Layer 2)
ρ : Density	7830		Kg/m^3	Effective material properties of composite are calculated by MAC code in Table 2.	
E : Elastic modulus	2.05e11		N/m^2		
υ : poisson ratio	0.3		-		
SigY : Yield stress	0.35e09		N/m^2		
Tangent modulus	0.636e09		N/m^2		
Hardening parameter	0 (Kinematic)		-		
Failure strain	0.25		-		
Orientation	Isometric		-	0º from x axis in local x-y plane	90º from x axis in local x-y plane
Layer thickness	0.0075	0.0075	m	0.015	0.015

Table 2 Effective composite material properties evaluated by the MAC code for zero levels of strain

	SiC	Ti-6Al-4V	(unit)		Composite
ρ : Density	3000	4428	Kg/m^3		3571.6
E1 : Axial elastic modulus	4.15e11	1.179e11	N/m^2		2.97e11
E2 : Transverse elastic modulus	4.15e11	1.179e11	N/m^2		2.48e11
υ12= υ13 : Axial poisson ratio	0.14	0.32			0.2066
υ23 : Transverse Poisson ratio	0.14	0.32			0.2493
G12=G13 : Axial shear modulus	182.05e09	44.65e09	N/m^2		93.010 e09
G23 : Transverse shear modulus	182.05e09	44.65e09	N/m^2		81.634e09
S11 : Axial tensile strength	5.9e09	1.38e09	N/m^2		3.36e09
S22=S33 : Transverse tensile strength	0.85e09	1.38e09	N/m^2		0.748e09
S12=S13 : Axial shear strength	0.425e09	0.480e09	N/m^2		0.370e09
S23 : Transverse shear strength	0.425e09	0.480e09	N/m^2		0.425e09
SC11 : Axial compressive strength	3.90e09	0.825e09	N/m^2		2.01e09
SC22=SC33 : Transverse compressive strength	3.90e09	0.825e09	N/m^2		1.04e09

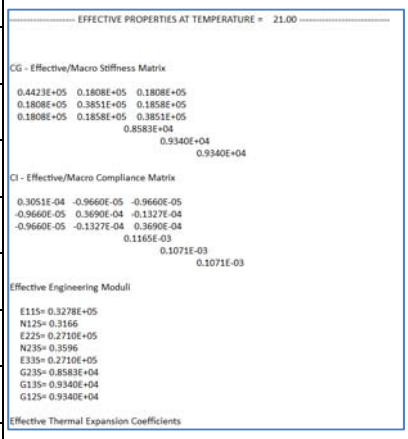

MAC/GMC Calculation Results

Two simulations are conducted by using the one-way coupling approach. The MAC code is used first for computing the equivalent material properties which correspond to zero levels of strain (Table 2). The LS-DYNA Lagrangian solver and the ABAQUS Explicit solver are then used for computing the response of the structure. The third solution is obtained by using the fully coupled MAC-ABAQUS explicit solution. The purpose of this analysis is to make certain that all three solutions give comparable results.

The pressure load time histories, computed by the BEST process, comprise the loading for all three structural analyses. Figure 16 presents typical load histories and the flow chart of the process that generate the loads for the structural analysis. Typical results computed by the LS DYNA and the ABAQUS solvers using the equivalent material properties, summarized in Table 2, are presented in Figure 17-(a) and 17-(b) respectively. Results from the fully coupled MAC-ABAQUS simulation are also presented in Figure 17-(c).

Figure 16 Interpret pressure loading for each solvers

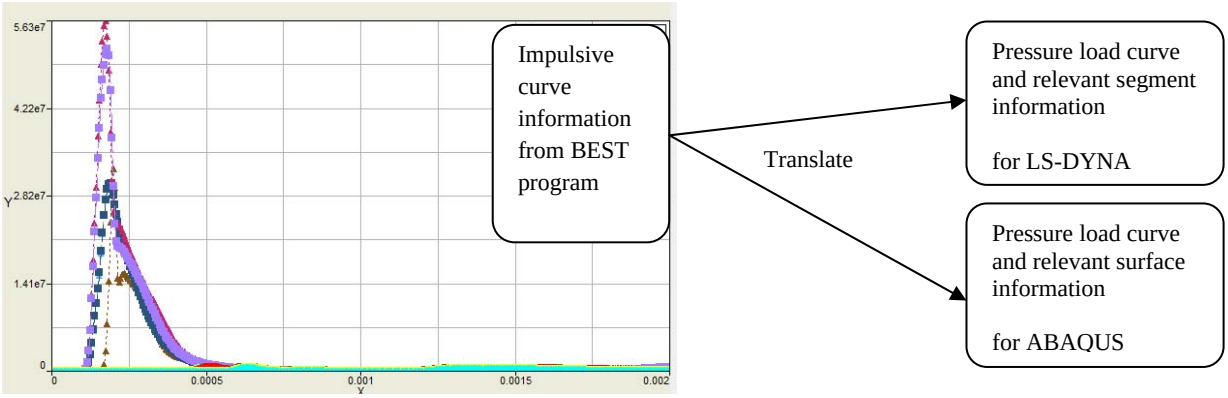

Figure 17 Structure response for standalone simulation using (a) LS DYNA; (b) ABAQUS/Explicit solver; (c) Fully coupled MAC-ABAQUS/Explicit

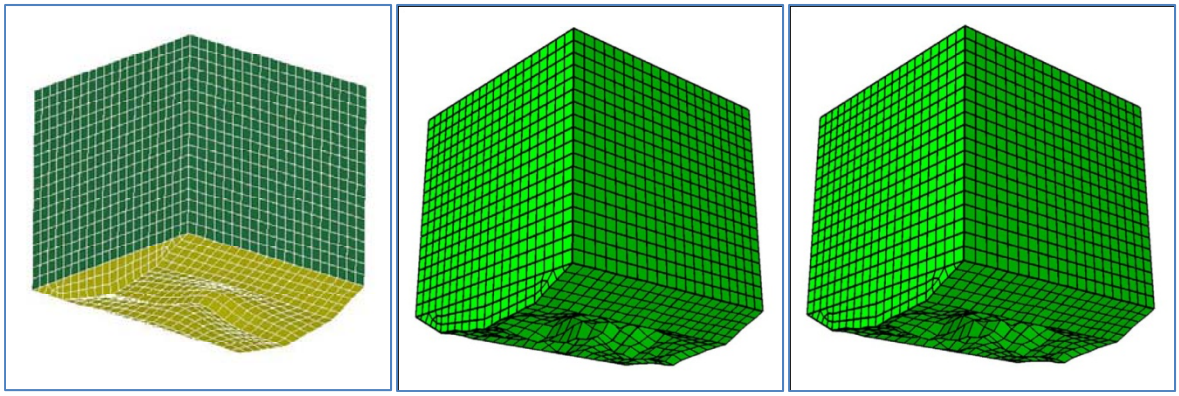

(a) (b) (c)

As it can be observed all three solutions produce comparable results. A similar tendency is demonstrated in the outer bottom response from all three solutions. Two valleys are created on either side with respect to the plane of symmetry along the y-direction and two peaks are created on both sides with respect to the plane of symmetry along the x-direction. For comparison, the vertical (z-displacement) of the center node and two valley points is presented in Figure 18 from the three analyses.

Figure 18 Z-displacement of the nodes.

(1-Standalone LS-DYNA solver; 2-Standalone ABAQUS solver; 3- Fully coupled MAC- ABAQUS solver)

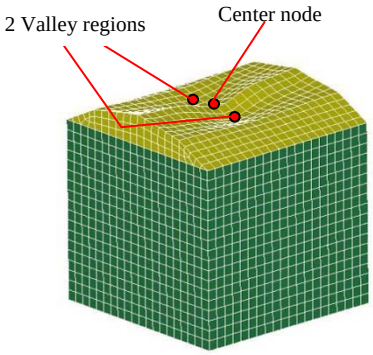

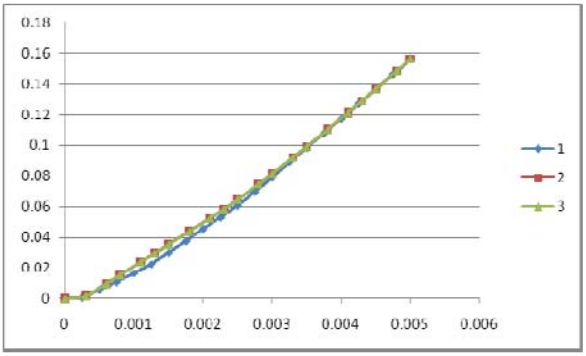

(a) Center node

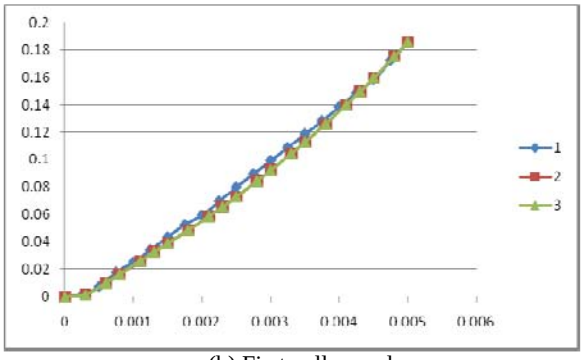

(b) First valley node

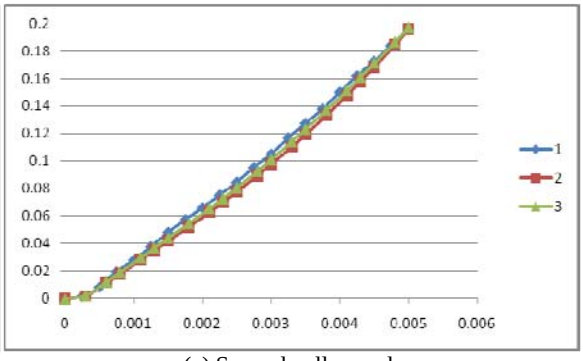

(c) Second valley node

The results of the comparison demonstrate almost identical values since element failure was not reached slightly larger z-displacement is encountered in the fully coupled MAC-ABAQUS simulation since effective material properties were updated continuously during calculation. The good agreement which is observed in the results summarized in Table 3 demonstrates the proper implementation and development of the fully coupled MAC-ABAQUS simulation capability.

Table 3 Summary of Z-displacement of the three representative nodes.

	Standalone 1 (LS-DYNA)	Standalone 2 (ABAQUS)	Fully coupled MAC-ABAQUS (ABAQUS)
Center node z-displacement (m)	0.1558	0.1559	0.1563
% increase of Standalone 1	-	0.06 %	**0.32 %**
% increase of Standalone 2	-	-	**0.26 %**

Valley node 1 z-displacement (m)	0.1854	0.1856	0.1867
% increase of Standalone 1	-	0.11 %	**0.70 %**
% increase of Standalone 2	-	-	**0.59 %**
Valley node 2 z-displacement (m)	0.1952	0.1957	0.1971
% increase of Standalone 1	-	0.25 %	**0.97 %**
% increase of Standalone 2	-	-	**0.97 %**

5 Case study about micro-level configuration of composite material

In order to demonstrate how the new multi-scale modeling methodology can be used for configuring light weight blast resistant armor, the target structure analyzed in the previous section is subjected to the combined load from 5.352kg of C4 and high velocity projectiles. An all steel configuration comprises the baseline design. The thickness of the four lateral sides and the roof is 0.01m, and the thickness of the inner floor and the outer V shaped bottom is 0.015m. The overall weight is approximately 2467kg. In this case study the micro-scale simulation capability is employed for identifying an inner floor and an outer V shaped shield configuration made out of composite that offers a similar level of protection with the steel structure. The relative composition of each composite laminate layer cell, the orientation of each laminate layer, and the thickness of each layer can be used as design parameters when determining a double floor configuration that weights less but offers similar protection levels with the one made out of steel. The level of permanent deformation and/or failure of the outer V shaped bottom and the maximum deformation encountered in the center of the inner floor comprise the performance metrics considered in this study. A configuration that reduces the total weight to 2222.3kg is identified. The outer V bottom structure has 0.03m thickness and the inner bottom thickness is 0.02m. The number of layers and the orientation of each layer are summarized in Table 4.

Table 4 Inner floor and outer V bottom configuration of re-designed composite floor

	Orientation		Thickness (m)	
	Inner floor	Outer V bottom	Inner Floor	Outer V bottom
Layer 1	0º from x axis in local x-y plane	0º from x axis In local x-y plane	0.010	0.015
Layer 2	90º from x axis in local x-y plane	90º from x axis in local x-y plane	0.010	0.015

The maximum deformation encountered in the composite outer floor is smaller compared to the steel structure (0.2348m vs 0.3279m). The overall deformation encountered in the two structures is presented in Figure 19. Further, the maximum displacement encountered in the middle of the inner floor is 4.289e-2m for the steel structure and 5.004e-3 for the composite. Thus, improved blast resistance characteristics are observed by the composite structure while the weight of the overall structure is reduced. This case study demonstrates how the multi-scale simulation can be used for configuring blast resistant light weight structures.

Figure 19 Deformation of steel (left) and composite (right) structures.

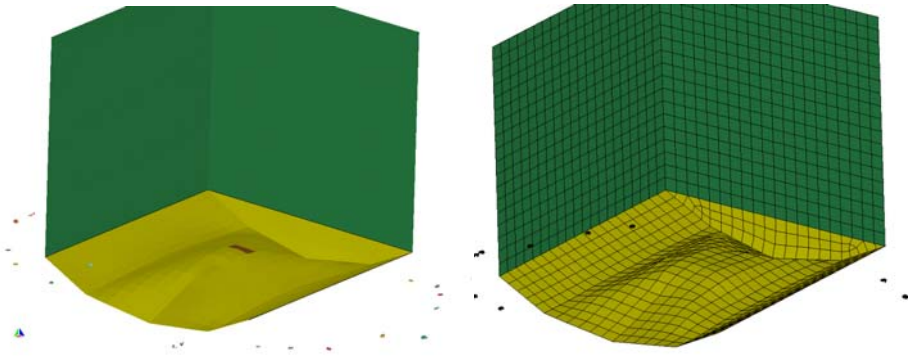

6 Conclusions

In this paper, a multi-scale approach for simulating blast events is presented and demonstrated. Readily available finite element solvers are combined to simulate the explosion of a buried explosive charge, the propagation of the shock wave through the soil and the air, the load from the shock wave on a target structure, and the response of the structure to the shock load. Since the ultimate objective is to design a vehicle with the safety of the occupants in mind, an ATD finite element model can be included as part of the vehicle finite element model in the simulations. Based on comparisons with test data, an ATD model can capture well the loads developed in the legs of an occupant during an explosion. Once confidence is established in the ability to conduct blast event simulations, multi-scale modeling for composites is integrated in the blast event simulations for inducing constitutive material properties of composites in the analysis and propagating information from the micro cell level to global structural level. The case study presented in this paper demonstrates how the multi-scale simulation capability allows using the composition of the composite and the layer arrangement of the composites for configuring composite structures exhibiting blast resistant characteristics similar to a steel structure, but at a reduced weight.

Acknowledgements

Part of the work presented in this paper has been supported by the Automotive Research Center, a U.S. Army Center of Excellence for Modeling and Simulation of Ground Vehicles led by the University of Michigan.

References

[1] Bell R. L., Hertel Jr. E.S., "A domain decomposition scheme for Eulerian shock physics codes," CED-Vol. 6, High Performance Computing in Computational Dynamics, ASME International Congress and Exposition 1994, pp. 67-72.

[2] Bergeron D., Walker R., and Coffey C., "Detonation of 100-gram anti-personnel mine surrogate charges in sand: A test case for computer code validation," Defense Research Establishment Suffield, SR668, National Defense, Canada, October 1998.

[3] Bird R., "Protection of vehicles against landmines," Journal of Battlefield Technology, Vol. 4, No. 1, March 2001.

[4] Fischer H., "United States Military Casualty Statistics: Operation Iraqi Freedom and Operation Enduring Freedom," Congressional Research Service Report number: RS22452, March 25, 2009.

[5] Galarneau M. R., Woodruff S. I., Dye J. L., Mohrle C. R., Wade A. L., "Traumatic brain injury during Operation Iraqi Freedom: findings from the United States Navy-marine Corps Combat Trauma Registry," Naval Research Health Center Report 06-25.

[6] Gupta A.D., Gregory F.H., Bitting R.L., and Bhattacharya S., "Dynamic analysis of an explosively loaded hinged rectangular plate," Computers & Structures, Vol. 26, pp. 339-344, 1987.

[7] Gupta A.D., Wisniewski H.L., and Bitting R.L., "Response of a generic vehicle floor model to triangular overpressure loads," Computers & Structures, Vol. 32, No. 3/4, pp. 527-536, 1989.

[8] Gupta A.D., "Dynamic Elasto-plastic response of a generic vehicle floor model to coupled transient loads," PVP-Vol. 351, Structures under Extreme Loading Conditions, ASME, pp. 81-86, 1997.

[9] Gupta A.D., "Estimation of vehicle floor plate loading and response due to detonation of a mine shallow-buried in dry sand and wet turf," US Army Ground Vehicle Survivability Symposium, Monterey, CA, Mar. 29 – April 1, 1999.

[10] Gupta A.D., "Modeling and analysis of a blast deflector for a tactical vehicle due to detonation of a mine buried in dry vs. saturated sand," US Army Ground Vehicle Survivability Symposium, 2002.

[11] Joachin C.E., McMahon G.W., Lunderman C.V., and Garner S.B., "Airblast Effects Research: Small-Scale Experiments and Calculations," Technical Report SL-99-5, August 1999, US Army Corps of Engineers.

[12] Kingery C., and Bulmarsh G., "Airblast parameters from TNT spherical air burst and hemispherical surface burst," ARBRL-TR-02555, US Army Ballistic Research Laboratory, Aberdeen Proving Grounds, MD, 1984.

[13] Laine, L., and Sandvik, A. Derivation of mechanical properties for sand. In 4th Asia-Pacific Conference on Shock and Impact Loads on Structures, Singapore, November 2001, pp. 361-368.

[14] McGlaun J.M., Thompson S.L., and Elrick M.G., "CTH: a three-dimensional shock wave physics code," Int. J. Impact Engng., Vol. 10, 1990, pp. 351-360.

[15] Sun J., Vlahopoulos N., Stabryla T. J., Goetz R., Van De Velde R., "Blast event simulation for a structure subjected to a landmine explosion," 2006 SAE Congress, SAE Paper 2006-01-0931.

[16] Westine P.S., Morris B.L., Cox B.L., and Polch E.Z., "Development of computer program for floor plate response from land mine explosions," Technical report No. 13045, US Army Tank-Automotive Command, Warren, MI, 1985.

[17] Williams K., and McClennan S., "A numerical analysis of mine blast effects on simplified target geometries: Validation of loading models," Defense R&D Canada-Valcartier, DRDC Valcartier TM 2002-260, 2002.

[18] Aboudi J., "Micromechanical analysis of composites by the method of cells," Appl. Mech. Rev. 42, 1989, 193-221.

[19] Aboudi J., "Mechanics of Composite Materials," Unified Micromechanical Approach, Elsevier, Amsterdam, 1991.

[20] Aboudi J., Pindera M. J., " Micro mechanics of metal matrix composites using the generalized method of cells model (GMC)," Mechanics of Materials 14, Elsevier, 1992, 127-139.

[21] Aboudi J., "Micromechanical Analysis of Thermo-inelastic multiphase short-fiber composites," Composite Engineering, Vol. 5, No.7, Elsevier, 1995, 839-850.

[22] Bednarcyk B. A., Pindera M. J., "An efficient implementation of the generalized method of cells for unidirectional, multi-phased composites with complex microstructures," Composites, Part B 30, Elsevier, 1999, 87-105.

[23] Bednarcyk B. A. and Pindera M. J., "Inelastic Response of a Woven Carbon/Copper Composite Part 2: Micromechanics Model," Journal of Composite Materials 34(4), 2000, 299-331.

[24] Steven M., Bednarcyk B. A., Hussain A., Katiyar V., "Micromechanics-Based Structural Analysis (FEAMAC) and Multi-scale Visualization Within Abaqus/CAE Environment," NASA/TM, 2010-216336.

[25] Pineda E. J., Waas A., Bednarcyk B. A., Steven M., Collier C. S., "Multiscale Failure Analysis of Laminated Composite Panels Subjected to Blast Loading Using FEAMAC/Explicit," NASA/TM, 2009-215813

[26] Zhang G., Hart C. J., Vlahopoulos N., Bishnoi K., Goetz R., Rostam F., "Simulation for the Response of a Structure Subjected to a Load from an Explosion," SAE World Congress & Exhibition, Apr 2008, Part 2.

[27] Bednarcyk B. A., Steven M., "MAC/GMC 4.0 Keywords Manual," NASA/TM – 2002-212077/Vol2.

[28] Bednarcyk B. A., Steven M., "FEAMAC Beta documentation,"

[29] ABAQUS User's Manual, Version 6.8, Dassault Systems, 2008.

[30] Jones R.M., "Mechanics of Composite Materials, 2nd Ed," Taylor and Francis, Inc., Philadelphia.

[31] Peters, S. T., Handbook of Composites, Chapman & Hall, 2nd ed, 1998.

[32] Bansal, N. P.; Handbook of Ceramic Composites, NASA Glenn Research Center, Kluwer Academic Publishers, 2005.